Notch and EGFR pathway interaction regulates neural stem cell number and self-renewal

Adan Aguirre[1,3], **Maria E. Rubio**[2], and **Vittorio Gallo**[1,*]

[1] Center for Neuroscience Research, Children's National Medical Center, Washington, DC 20010

[2] University of Pittsburgh Medical School, Department Otolaryngology, Pittsburgh, PA 15261

Abstract

Specialized cellular microenvironments, or "niches," modulate stem cell properties, including cell number, self-renewal and fate decisions[1,2]. In the adult brain, niches that maintain a source of neural stem cells (NSCs) and neural progenitor cells (NPCs) are the subventricular zone (SVZ) of the lateral ventricle and the dentate gyrus of the hippocampus[3–5]. The size of the NSC population of the SVZ at any time is the result of several ongoing processes, including self-renewal, cell differentiation, and cell death. Maintaining the balance between NSC and NPCs in the SVZ niche is critical to supply the brain with specific neural populations, both under normal conditions or after injury. A fundamental question relevant to both normal development and to cell-based repair strategies in the central nervous system is how the balance of different NSC and NPC populations is maintained in the niche. EGFR and Notch signaling pathways play fundamental roles during development of multicellular organisms[6]. In *Drosophila* and in *C. elegans* these pathways may have either cooperative or antagonistic functions[7–9]. In the SVZ, Notch regulates NSC identity and self-renewal, whereas EGFR specifically affects NPC proliferation and migration[10–13]. This suggests that interplay of these two pathways may maintain the balance between NSC and NPC numbers. Here we show that functional cell-cell interaction between NPCs and NSCs through epidermal growth factor receptor (EGFR) and Notch signaling plays a crucial role in maintaining the balance between these cell populations in the SVZ. Enhanced EGFR signaling in vivo results in the expansion of the NPC pool, and reduces NSC number and self-renewal. This occurs through a non-cell-autonomous mechanism involving EGFR-mediated regulation of Notch signaling. Our findings define a novel interaction between EGFR and Notch pathways in the adult SVZ, and thus provide a mechanism for NSC and NPC pool maintenance.

We examined whether changes in SVZ NPC number affect NSC properties. In the *CNP*-hEGFR mouse, the hEGFR is expressed in *CNP*-expressing NPCs and in NG2$^+$ progenitors[14–15], but not in *GFAP*-expressing NSCs or in neuroblasts (Sup.Fig. 1a,b).

---

*Corresponding Author: Dr. Vittorio Gallo, Center for Neuroscience Research, Children's National Medical Center, 111 Michigan Ave. NW, Washington, DC 20010, Phone: 202-476-4996, Fax: 202-476-4988, vgallo@cnmcresearch.org.
[3]Present Address: SUNY at Stony Brook University, Pharmacology Department, Stony Brook, NY 11794-5140

EGFR overexpression enhances EGFR signaling in the adult SVZ (data not shown) and expands the NPC pool[14–15] (Sup.Fig. 1a,b). The SVZ of *CNP*-hEGFR mouse contains more NG2^{+} progenitors than WT, but a reduced number of GFAP[+] NSCs (Fig. 1a; Supplementary Fig. 2). In WT, GFAP^{+} cells exhibit a radial glia-like morphology (Sup.Fig. 1c1), whereas in *CNP*-hEGFR mice GFAP^{+} cells display a morphology of protoplasmatic astrocytes (Sup.Fig. 1d1)[16]. GFAP and Nestin were co-expressed in the WT SVZ, while the percentage of GFAP[+]Nestin^{+} cells was reduced in *CNP*-hEGFR mice (Fig. 1a,b).

In SVZ cells from *CNP*-hEGFR mice, Lex[+]Nestin[+]GFAP[+] NSCs were reduced, compared to WT (Fig. 1a,b). This was not due to cell death (0.6+/−0.02 and 0.5+/−0.06% of Caspase3^{+} cells/10^6 um^3, WT and *CNP*-hEGFR, respectively). Ultrastructural analysis[17] confirmed fewer NSCs and more neuroblasts in *CNP*-hEGFR mice compared to WT (Sup.Fig. 3).

We used LeX antibodies[18,19] to FACS-purify LeX[+]*CNP*-EGFP[neg] SVZ NSCs from *CNP*-EGFP and *CNP*-EGFP/*CNP*-hEGFR mice (Sup.Fig. 4). LeX[+]*CNP*-EGFP^{neg} cells were GFAP[+] (data not shown). The number of LeX[+]*CNP*-EGFP[neg] NSCs was reduced in the *CNP*-hEGFR mouse, whereas LeX[+]*CNP*-EGFP[+] NPCs were increased (Sup.Fig. 4). LeX[+]*CNP*-EGFP[neg] NSCs from *CNP*-hEGFR mice displayed a reduction in LeX[+] neurosphere[19,20] number and size, compared to WT cells (Fig. 1c,d). Conversely, *CNP*-EGFP[+]LeX[+] NPC proliferation was increased (not shown).

In *GFAP*-GFP/*CNP*-hEGFR mice, *GFAP*-GFP^{+} cells with radial glia-like morphology were almost absent in the SVZ (Sup.Fig. 5b). Conversely, in *GFAP*-GFP mice, GFP^{+} cells displayed radial glia-like cell morphology throughout the SVZ (Sup.Fig. 5a). In FACS-purified cells from *GFAP*-GFP and *GFAP*-GFP/*CNP*-hEGFR mice, enhanced EGFR signaling reduced the number of LeX[+]*GFAP*-GFP[+] NSCs, whereas the number of LeX[+]*GFAP*-GFP[neg] NPCs was increased (Sup.Fig. 5c,d). NSCs from *GFAP*-GFP/*CNP*-hEGFR mice displayed reduced neurosphere number and size compared to cells from *GFAP*-GFP mice (Sup.Fig. 5c,d), however proliferation of LeX[+]*GFAP*-GFP[neg] NPCs was increased (not shown). These results show that enhanced EGFR signaling and expansion of SVZ *CNP*-expressing progenitors[14,15] reduces the number, proliferation, and self-renewal of *GFAP*-expressing NSCs.

Notch[10,21,22], BMP[23,24] and Shh[25] regulate NSC properties in the SVZ. Enhanced EGFR signaling upregulated genes involved in neurogenesis [Sup. Table 1 (GEO access number GSE21913) and Fig. 2a], whereas Notch signaling elements were downregulated. Shh and BMP pathways were not modified (data not shown). In WT and *CNP*-hEGFR SVZ Notch1 was mainly detected in NSCs[22,26], whereas Dll1 and Jagged1 were detected in NPCs and in neuroblasts (Sup.Fig. 6a–f; see also Fig. 4a–d). *Dll*-EGFP electroporation demonstrated expression in EGFR[+]NG2^{+} and in Dcx^{+} cells, but not in GFAP^{+} cells (Sup.Fig. 6g–j). Conversely, *Hes1* activity was mainly observed in GFAP^{+} cells (Sup.Fig. 6k–m; see also Fig. 4a–d). Notch1, NICD, Dll1, RBPJK and Hes1 proteins were decreased by 60 ± 3, 63 ± 4, 20 ± 2, 30 ± 2.5 and $40 \pm 3\%$ upon enhanced EGFR function, respectively (n= 3–4 each; Fig. 2a). Conversely, Numb was increased by $45 \pm 3\%$ (n=3). In the SVZ of the Wa2

mouse14, NPC number and proliferation were reduced27, and Notch1, NICD, RBPJK and Hes1 were upregulated, as compared to WT (Fig. 2b).

EGF infusion into the lateral ventricle of *GFAP*-GFP mice increased the number of BrdU$^+$ cells in the SVZ, downregulated Notch signaling and expanded EGFR-expressing NPCs (Sup.Fig. 7a-e). Proliferation and self-renewal of NSCs from EGF-infused SVZ were reduced compared to controls (Sup.Fig. 7f,g).

To rescue the NSC phenotype in the postnatal *CNP*-hEGFR mice, we overexpressed the constitutively active form of Notch1 (Notch1 intracellular domain; NICD) in *CNP*-hEGFR SVZ cells (Sup.Fig. 8a). Neurosphere numbers and size were greater in *NICD*- than in mock-transfected cells (Sup.Fig. 8b). *NICD* electroporation in SVZ cells of *CNP*-hEGFR/ *GFAP*-GFP mice partially rescued the radial glia-like morphology of *GFAP*-expressing cells (Fig. 2c,d; see also Fig. 4a1–a3 and b1–b3), and increased neurosphere number and size (Fig. 2e,f). After adenovirus-mediated transduction of *NICD* (Fig. 2g) in adult WT and *CNP*-hEGFR mice, NICD levels were higher (30 ± 3%) in *NICD*-LacZ- (ad-*NICD*) than in LacZ adenovirus (Ad-LacZ)-infected SVZs, whereas Numb levels were reduced (55 ± 4%) (Fig. 2h). *NICD* transduction rescued NSC properties in the SVZ of *CNP*-hEGFR/*GFAP*-GFP mice (Fig. 2h,i).

We infused cytosine-β-D-arabinofuranoside (Ara-C) into the LV to deplete dividing NPCs9. In saline-perfused adult mice, BrdU$^+$ cell number was significantly higher in *CNP*-hEGFR mice (24.1+/–2.1 cells/10^6 μm^3) compared to WT (12.4 +/–0.5 cells/10^6 μm^3) (Sup.Fig. 9a,b; *t*-test p<0.008), whereas NSC number was reduced (Sup.Fig. 9a,b, and Fig. 3a; *t*-test p<0.005). Ara-C increased GFAP$^+$ cell number in the SVZ of adult *CNP*-hEGFR mice (Sup.Fig. 9c,d and Fig. 3a). We observed higher levels of Notch1 in GFAP$^+$ NSCs of Ara-C-treated *CNP*-hEGFR and WT mice, compared with saline-infused mice (not shown). In *CNP*-hEGFR mice, *Hes1* and *RBPjk* mRNAs and Notch1 protein levels were higher in Ara-C-treated SVZ tissues than in saline controls (Fig. 3b), whereas *Numb* mRNA and protein were reduced (Fig. 3b). Cell proliferation and self-renewal were enhanced in neurospheres from Ara-C-treated tissue, compared with saline (Fig. 3c). Altogether, these data indicate that NPCs regulate NSC proliferation and self-renewal in vivo.

To demonstrate that contact with NPCs regulates NSC proliferation and self-renewal through Notch, we co-cultured confluent SVZ NPCs from WT or *CNP*-hEGFR mice with NSCs FACS-purified from *GFAP*-GFP mice (Sup.Fig. 10). *GFAP*-GFP$^+$ NSCs were then FACS-purified from these co-cultures. Notch signaling was downregulated in NSCs co-cultured with *CNP*-hEGFR NPCs, and cell proliferation and self-renewal were reduced (Fig. 3d and Sup.Fig. 10c). NICD transduction partially rescued this phenotype (Fig. 3d). In NSCs FACS-purified from Wa2 NPC/WT NSC co-cultures Notch signaling and neurosphere formation were enhanced, as compared to WT NPC/WT NSC in NSCs (Fig. 3e and Sup.Fig. 10f). These results confirm that EGFR regulates Notch through a non-cell-autonomous mechanism.

We determined whether EGFR regulates the Notch pathway and investigated the molecular mechanism. In transfected SVZ cells, *CBF-1* and *Hes1* promoter activity was higher in WT

than in *CNP*-hEGFR cells, even after *NICD* co-transfection (Sup.Fig. 11a). In WT cells, *Hes1* activity was enhanced by *NICD* and reduced after *hEGFR* co-transfection (Sup.Fig. 11b). *hEGFR* co-transfected with different *Notch* constructs (Sup.Fig. 11c) reduced *Hes1* activation (Sup.Fig. 11d), and the EGFR inhibitor PD16839315 restored *Hes1* activity (Sup.Fig. 11e). *CNP*-hEGFR cells plated on WT cells transfected with *Hes1*-luciferase suppressed basal *Hes1* activity; this effect was reversed by PD168393 (Sup.Fig. 11f). Finally, *Hes1* promoter activity was higher in Wa2 SVZ cells than in WT cells (Sup.Fig. 11g).

We electroporated Notch target constructs (Sup.Fig. 12) to identify SVZ Notch-responsive cells and to elucidate the mechanism of Notch regulation. *Hes1* activity was observed in NSCs (Fig. 4a-d and Sup.Fig. 12m,n), and was found in a larger percentage of *GFAP*-GFP$^+$ cells (47.8+/−3.6 cells/μm3) than in *GFAP*-GFP$^+$/*CNP*-hEGFR$^+$ cells (23.6+/−4.6 cells/μm3, p<0.01). Similar results were observed with *CBFRE*-GFP and *Hes5*-GFP (Sup.Fig. 12a–l; o–r). *Hes1* activity in NSCs of *GFAP*-GFP/*CNP*-hEGFR mice was rescued by *NICD* co-electroporation (66.5+/−71 cells/μm3, p<0.01; n=4). In Wa2 mice, a larger percentage of SVZ NSCs displayed *Hes1* and *CBFRE* activity, compared to WT (Sup.Fig. 13a–c, and not shown). shRNA-mediated knockdown of *hEGFR* in *CNP*-hEGFR mice in vivo caused upregulation of Notch1 and Hes1 (Sup.Fig. 13d,e). Consistent with these results, Dll-EGFP electroporation revealed a larger percentage of *Dll*-EGFP$^+$ cells in the SVZ of the WT mouse, compared to *CNP*-hEGFR mouse (Sup.Fig. 14). Altogether, our findings demonstrate that EGFR is an upstream regulator of Notch through a non-autonomous cellular mechanism.

Numb interacts with E3 ubiquitin ligases to regulate Notch receptor degradation[28]. Changes in Notch signaling levels directly regulate Numb expression[29]. Figure 4e shows that *NICD* overexpression reduced Numb in SVZ cells, whereas EGFR overexpression upregulated Numb, and reduced Notch1 and NICD levels. The Notch inhibitor DAPT upregulated Numb (Fig. 4f).

We determined the extent of Numb/Notch1 interaction in the SVZ by immunoprecpitation assays. Higher levels of Notch1 associated with Numb in *CNP*-hEGFR samples, compared to WT (Fig. 4g1). Anti-ubiquitin immunoprecipitation followed by anti-Notch1 immunoblotting demonstrated higher levels of Notch ubiquitination in *CNP*-hEGFR mice (Fig. 4g2). Stereotaxic injection in WT and *CNP*-hEGFR mice with either Ad-LacZ or *NICD*-LacZ adenovirus showed that both Numb/Notch interaction and Notch1 ubiquitination were reduced after NICD transduction (Fig. 4h).

To demonstrate that EGFR signaling promotes Notch ubiquitination via Numb, we performed gain- and loss-of-function experiments in SVZ cultures. After EGFR transfection, we observed increased Numb levels and reduced NICD expression, compared to the mock construct (Fig. 4i). PD168393 reversed this effect (Figure 4i). EGFR overexpression in WT cells promoted Numb and Notch association and enhanced Notch1 ubiquitination (Fig. 4j). siRNA-mediated EGFR knock down in *CNP*-hEGFR SVZ cultures reduced Numb and Notch1 interaction (Fig. 4k1), and decreased Notch1 ubiquitination (Fig. 4k2).

To confirm the role of EGFR and Numb in inhibiting Notch, we analyzed *Hes1* promoter activity by co-transfection in WT SVZ cells with a *Hes1*-luciferase reporter construct, along with *hEGFR* and *Numb* expression vectors. *Hes1* activity was activated only by the *NICD* construct (Sup.Fig. 11h). However, *Numb* blocked *NICD* and reduced *Hes1* activity (Supplementary Fig. 11h). *Hes1* activity was further reduced by co-transfection with *NICD*, *Numb*, and *hEGFR* (Sup.Fig. 11h). Finally, siRNA mediated knockdown of *Numb* in vivo caused upregulation of *Notch1* and *Hes1* activity (Fig. 4l–o). Scrambled siRNA electroporation in vivo showed that *Hes1* activity was present in a small percentage of GFAP$^+$ and Nestin$^+$ NSCs (Fig. 4n; 3.9+/−0.51 cells/μm3), however after *Numb* knock down *Hes1* activity was present in a larger percentage NSCs (Fig. 4o; 7.1+/−0.56 cells/μm3, p<0.01; n=4). Together, these results demonstrate that EGFR signaling reduces Notch activation through Numb-dependent Notch1 ubiquitination.

Our results point to an interaction between two signaling pathways -EGFR and Notch - that play fundamental and selective roles in the maintenance of NSCs and NPCs in the SVZ niche. This interplay occurs through the direct interaction between NPCs and NSCs, demonstrating the existence of a cellular homeostatic mechanism that involves two specific molecular pathways. Our study also proves that altering particular signaling mechanisms in selective cell types of the SVZ can cause profound changes in the overall cell composition of this neurogenic region of the adult brain. Defining interactions and homeostatic mechanisms that occur between different types of SVZ cells under normal conditions provides crucial information on possible alterations of specific signaling pathways that might occur under pathological conditions or after brain injury.

METHODS SUMMARY

Generation/genotyping of *CNP*-hEGFR, *hGFAP*-GFP and Wa2 mice was performed as described14,15. Wild-type C57/Bl6 and FVB/N mice were used as controls. Histology, immunohistochemistry and EM studies were performed on fresh floating or vibratome sections as described previously19,20. Immunohistochemestry and confocal imaging were used to characterize the SVZ cell composition of the postnatal and adult brain. Image analysis, three-dimensional rendering, and cell counting were done in Photoshop (Adobe) and ImageJ software. NSCs and NPCs were isolated and characterized by FACS sorting using CD15, GFAP, EGFR and NG2 antibodies. Cell proliferation, self-renewal and biochemical analysis were performed from FACS-purified cultured cells and SVZ tissue. To compare SVZ expression profiles of genes involved in NSC development/neurogenesis in *CNP*-hEGFR and WT mice, we performed gene array (SuperArray, Bethesda, MD) expression on spotted cDNA fragments encoding 250 mouse genes. To monitor Notch-signaling pathway in the postnatal SVZ of the CNP- and WT mice, mouse brains were electroporated using the ECM 830 BTX electroporator (Harvard Apparatus, Holliston, MA). Each electroporation result was reproduced in multiple brains derived from at least three separate litters. SVZ NPC cell depletion using Ara-C (2%, Sigma) in vehicle (0.9% saline) or vehicle alone was performed as previously described3. EGF (100nm/ul, Upstate) in vehicle (0.9% saline), or vehicle alonewas infused into the LV of adult *GFAP*-GFP and WT mice (infusion coordinates: anterioposterior, 0; lateral, 1.1; dorsoventral, 1.5 mm medial to lateral relative to bregma) for 5 days using micro-osmotic pumps (Alzet, model 1007).

Brains were then processed for FACS-purification, cell culture or histology. At least 3 different brains for each strain and each experimental condition were analyzed and counted. Cell counting was performed blindly and tissue sections were matched across samples. The analysis of the SVZ was performed at different anterior-posterior and dorso-ventral levels of the lateral ventricle. Statistical analysis was performed by unpaired t-test.

METHODS

Animals

Details on the generation and characterization of *CNP*-hEGFR transgenic mice have been previously reported[30,15]. Genotyping of the mice was performed by PCR[15]. Robust hEGFR expression was detected in total brain and spinal cord lysates from adult brain by using monoclonal anti-human EGFR antibody to probe Western blots after immunoprecipitation with a polyclonal anti-EGFR antibody[14,15,30]. Consistent with the idea that the CNP promoter drives expression in OLs, hEGFR expression was detected in OL lineage cells of the SVZ, white matter and cerebral cortex in P8-P90 CNP-hEGFR mice, and in $NG2^+$ progenitor cells of the SVZ[15]. Transgenic mice were backcrossed >4 generations onto C57BL/6. In the *CNP*-hEGFR mouse strain, the *CNP* promoter drives expression in NPCs and in the entire oligodendrocyte lineage; hEGFR expression was detected at both P8 and P90 in $NG2^+$ progenitors of the SVZ, and in $NG2^+$ progenitors and oligodendrocytes of the white and gray matter[14,15]. The mouse strain expressing the *hGFAP*-EGFP (kind gift of F. Kirchhoff, Max Planck Institute of Experimental Medicine, Goettingen, Germany) was previously characterized[31]. The EGFR-mutant mouse (waved-2 mutation; Wa2)[32] was obtained from Jackson Labs (Bar Harbor, ME). All animalprocedures were performed according to the Institutional Animal Care and Use Committee of Children's National Medical Center and the National Institutes of Health "Guide for the Care and Use of Laboratory Animals."

Immunohistochemistry and antibodies

Freshly cut, floating tissue sections (20–40μm) from P8 and P90 mice were prepared as previously described[14,15]. Primary antibody dilutions were: 0.5μg/ml for the specific anti-hEGFR (Biofluids, Caramillo, CA); 1:500 for anti-BrdU (Accurate, Westbury, NY), anti-NG2 antibody (Chemicon, Temecula, CA), monoclonal anti-GFAP (mouse monoclonal, Sigma Aldrich, St. Louis, MO), polyclonal anti-GFAP (rabbit polyclonal, Covance, Berkeley, CA), anti-S100β (DAKO, Denmark; rabbit anti-human clone A5110), and anti-Nestin (Chemicon); 1:50 for anti-LeX (MMA clone, BD Biosciences, San Jose, CA), anti-full length Notch-1, Jagged1, Delta like-1 (Dll) and anti-NICD (from Developmental Studies Hybridoma Bank, Iowa, IA).

BrdU administration

The BrdU labeling protocol was performed as previously described[33,19]. The number of proliferating progenitor cells in the subependyma of the lateral ventricle was determined following short-term (2h), or long-term (30d) retention. Mice were injected intraperitoneally with a single dose of BrdU (50 μg/g body weight) every 3h for five injections and were sacrificed either 1h or 30d after the final injection.

Conventional transmission electron microscopy

Wild type and *CNP*-EGFR mice (P8, n=6 for each phenotype; adult, n=4 for each phenotype) were perfused through the heart with a mixture of 3% paraformaldehyde and 1.25% glutaraldehyde in 0.1M phosphate buffer (PB). Brains were removed and postfixed overnight with the same fixative. Brains were sectioned with a vibratome and stored in 0.1M PB. Before postfixation for 1 hour with 1% osmium tetroxide, slices were washed in 0.1M cacodylate buffer pH7.2. After, brain slices were dehydrated through a series of ethanol solutions (50%, 70%, 85%, 95% and 100%), infiltrated with epoxy resins and flat embedded. Sections with the lateral ventricle and the SVZ were trimmed and mounted on blocks and cut with an ultramicrotome. Ultrathin sections (70–80 nm in thickness) were counterstained with uranyl acetate and lead citrate and analyzed with a TECNAI G2 Spirit Biotwin TEM (FEI, Hillsboro, OR, USA). The images were captured with an AMT XR40 4 megapixel side mounted CCD camera (Danvers, MA, USA) using the electron micrograph montage option. Image processing was performed with Adobe Photoshop using only the brightness and contrast commands. The identification of cell types in the lateral wall of the lateral ventricle and SVZ was performed on electron micrographs following well-described ultrastructural criteria by Doetsch et al. (1997). Cells were false colored and were counted manually.

Microarray and PCR analysis

GEArray™ expression array systems (cat #OMM-404MM and #OMM-404MM, SuperArray, Bethesda, MD) consisting of spotted cDNA fragments encoding 250 mouse genes involved in NSC development/neurogenesis and in Nocth signaling, as well as control sequences (PUC18, glyceraldehyde-3-phosphate dehydrogenase (GAPDH), peptidylpropyl isomerase A (Ppia), and b-actin) were employed to compare gene expression between WT and *CNP*-hEGFR SVZ tissue. Total RNA was isolated with theTrizol method (Invitrogen) and further processed for microarray hybridization according to the manufacturer's instructions. The arrays were visualized by autoradiography and hybridization signals were scanned and analyzed for density in GEArray Expression Analysis Suite 2.0. The normalized value for each gene was calculated by dividing the value of each gene by the average value of the housekeeping genes GAPDH, Ppia, and β-actin.

For RT-PCR, RNA was isolated from P8 and P90 SVZ tissue or from FACS-purified SVZ cells (WT and *CNP*-hEGFR mice), using Trizol (Invitrogen). RNA (1μg) from each sample was reverse-transcribed using the SuperScript™ First-Strand cDNA Synthesis kit (Invitrogen). The mouse gene-specific primers were obtained from Integrated DNA Technologies, Inc. (Coralville, IA). Primer sequences for PCR analysis are found in Supplementary Experimental Procedures. Genes were amplified by denaturation at 94°C for 1 min, annealing at 60°C for 1 min, and extension at 72°C for 1 min for 28 cycles. PCR products were resolved by 1.2% agarose gel electrophoresis and visualized by ethidium bromide staining.

In vivo electroporation

For gene transfer into postnatal SVZ cells, *GFAP*-GFP and *GFAP*-GFP/*CNP*-hEGFR P2-P3 pups were injected with 1–2μg of pFLAG-NICD (gift from Dr. Raphael Kopan),

shhumanEGFR (GeneCopoeia, Cat #HSH004605-LvH1, access number NM_005228.3; HSHH004605 actcactctccataaatgc; HSH004605-2 cgtcagcctgaacataaca; HSH004605-3 gaccagacaactgtatcca; HSH004605-4 ccgtcgctatcaaggaatt), *CAG*-GFP and *Hes1*-dsRED and *Hes1*-GFP (gift from Dr. Cepko L. Constance)34 CBFRE-EGFP (gift from Dr. Nicholas Gaiano)22, *Dll*-GFP (gift from Richard Grosschedl)35 and *Hes5*-GFP (gift from R. Kageyama)36 DNA into the LV, followed by electroporation (100V/50ms, five times at 950ms intervals; the angle of the paddles was adjusted to 20–40 degrees) using an ECM 830 BTX electroporator (Harvard Apparatus, Holliston, MA).

In vivo viral labeling

SVZ cells were infected using a Notch Intracellular domain (Ad-NICD) or control (Ad-LacZ) construct Adenovirus (gift of Dr. Igor Prudovsky) by direct injection into the LV. Adenovirus production and titer determination were previously described37. P90 WT and *CNP*-hEGFR mice were injected with the Adenovirus stock (2μl; titer of $2–4 \times 10^6$ cfu/ml). Injections were performed stereotaxically at the following coordinates (anterioposterior relative to bregma, mediolateral, and dorsoventral from surface of the brain) for epl-SVZ (0, 1.8, 3.0mm). Brains were processed for histology at 2, 7, 14 and 28 days after infection, and sections were immunostained for NICD, GFAP, S100b, NG2 and BrdU antibodies.

FACS sorting and cell culture

FACS-purification of LeX$^+$NG2$^-$/EGFP^{neg} (NSCs) in the *CNP*-EGFP mouse or GFAP-GFP$^+$LeX$^+$NG2^{neg} (NSCs) in the *GFAP*-GFP mouse has been previously described19. Tissue from P8 *CNP*-hEGFR, *CNP*-EGFP/*CNP*-hEGFR, *GFAP*-GFP or *CNP*-hEGFR/ *GFAP*-GFP mice was dissociated into single cell suspensions, followed by immunostaining for NG2 and LeX (MMA clone)19. SVZ neural stem cells and NPCs (after EGF or saline infusion, or 5–7days after focal demyelination of the corpus callosum) were FACS-purified using anti-LeX antibodies to purified LeX$^{+/}$*GFAP*-GFP$^+$ (NSCs) or *GFAP*-GFP^{neg}LeX$^+$ (NPCs) cells from the *hGFAP*-GFP mouse. Tissue was dissociated into single cell suspensions, followed by immunostaining for NG2 and LeX (MMA clone)19. To FACS-purify NSCs, antibodies were used in combination with appropriate R-PE- and PE-Cy5.5-conjugated secondary antibodies (Caltag, Burlingame, CA). Cell suspensions were analyzed for light forward and side scatter using a FACSAria instrument (BD, Biosciences, Franklin Lakes, NJ).

Cultures of FACS-purified cells have been previously described19. FACS-purified NSCs were seeded at a density of 10 viable cells/μl on uncoated 24-well plates (BD Falcon, Franklin Lakes, NJ), and grown in SCM for 6 days in vitro (DIV) with daily addition of 20ng/ml EGF and 10ng/ml bFGF (Upstate, Charlottesville, VA)19,20. Primary neurosphere colonies were subcloned to assay NSC self-renewal by mechanical dissociation and replated at a density of 10cells/μl on uncoated 24-well plates. It is important to note that in Supplementary Figure 6 neurosphere analysis was performed starting with the 2nd passage. This was done to overcome the experimental limitations due to low number of cells recovered after FACS.

SVZ micro-dissection

SVZ areas were micro-dissected from 300μm-thick brain coronal sections. Single cell were dissociated19,38 on coated coverslips in 24-well plates (BDFalcon, Franklin Lakes, NJ). Coverslips were processed for immunocytochemistry 2h after plating.

Western blots and immunoprecipitation

SVZ tissue (WT and *CNP*-hEGFR mice) was micro-dissected from 300μm-thick coronal sections of P8 and P90 brains, and used for protein extraction using lysis buffer (50mM Tris-HCl, pH7.5, 1mM EDTA, 1mM EGTA, 1mM sodium orthovanadate, 50 mM sodium fluoride, 0.1% 2-mercaptoethanol, 1% triton X-100, plus proteases inhibitor cocktail; SIGMA). Protein samples (20μg) were separated on GENE Mate express Gels 420% (ISC BioExpress, Kaysville, UT) and transferred to PVDF membranes (Millipore, Bedford MA). Numb, Notch1, NICD, Dll1, Hes1, RBPjk, ubiquitin, and actin proteins, were detected using an enhanced chemiluminescence substrate mixture (ECL Plus, Amersham, Buckinghamshire, UK). Selective primary antibodies from Santa Cruz Biotechnologies (Caramillo CA) were used at 1μg/ml. Antibodies were used in combination with a secondary horseradish peroxidase-conjugate (Santa Cruz Biotechnologies).

For immunoprecipitation, SVZ tissue extracts from WT and CNP-hEGFR mice were prepared in RIPA buffer containing. Aliquots (200μg protein) were incubated overnight with antibodies against ubiquitin (Santa Cruz Biotechnology), Numb or Notch1 and 15μl of Agarose A (Santa Cruz Biotechnology). Immunocomplexes bound to agarose A were collected by centrifugation and washed twice in 500μl RIPA buffer containing inhibitors. Precipitated proteins were analyzed by immunoblotting. Bands were detected using HRP and developed with a chemiluminescent substrate (ECL, Amersham).

Ara-C and EGF infusion

Ara-C (2%, Sigma) in vehicle (0.9% saline) or vehicle alonewere infused onto the surface of the brain of adult mice (coordinates: anterioposterior, 0, lateral, 1.1, dorsoventral, 1.5mm medial to lateral relative to bregma) for 6 days with micro-osmotic pumps (Alzet, model 1007) as previously described by Doetsch et al. (1999). EGF (100nm/ul, Upstate) in vehicle (0.9% saline), or vehicle alone was infused into the LV in adult *GFAP*-GFP and WT mice (infusion coordinates: anterioposterior, 0; lateral, 1.1; dorsoventral, 1.5 mm medial to lateral relative to bregma) for 5 days using micro-osmotic pumps (Alzet, model 1007). Mice were then processed for FACS-purification, cell culture or histology.

Plasmids, siRNAs, cell transfection and luciferase assays

SVZ tissue was dissected from 300μm-thick brain sections prepared from P8 WT and *CNP*-hEGFR brains and processed for cell culture19. After SVZ dissection and single cell dissociation, cells were plated in 12-well cell culture dishes at a density of 50 cells/μl for 24 hours. At the time of transfection, cell cultures were approximately 60% confluent. Cell transfections were performed using the NeuroPORTER Transfection reagent (Genlantis, San Diego, CA) following manufacturer's instructions. The cell permeable, irreversible EGFR blocker (PD168393, Calbiochem, La Jolla, CA), was used 24hrs after cell transfection. Cells

were pre-incubated with PD168393 (PD) for 4hrs at 37°C in 5% CO_2 and then medium was changed to fresh SCM.

A commercially available siRNA directed toward the hEGFR was purchased from Dharmacon (SMARTpool Cat. No. L-003114-00, Locus NM_201283; sequence J-003114-10, CAAAGUGUGUAACGGAAUA; J-003114-11, CCAUAAAUGCUACGAAUAU, J-003114-12, GUAACAAGCUCACGCAGUU, J-003114-13, CAGAGGAUGUUCAAUAACU. and siRNA directed toward the mNumb (Santa Cruz Biotechnologies Inc. Cat. No. sc-42147; Locus NM_010949, 110 GUAGCUUCCCAGUUAAGUAtt, 412 CGAUGGAUCUGUCAUUGUUtt, 884 CCCUACGCAUCAAUGAGUUtt). siRNA transfection produced selective knockdown of the hEGFR and mNumb. Briefly, 2μl of 20pM of siRNA solution and 12μl of the transfection reagent were incubated in 100μl of SCM for 20 minutes, in order to facilitate complex formation. The siRNA transfection mix was added to the SVZ cells cultured in 2.5% FBS. Controls consisted of non-specific siRNA. SVZ cells were transfected for 7 hours at 37°C, washed with Hanks' buffer and cultured in SCM 2.5% FBS for an additional 24 hours. The medium was then changed to basal SCM (20 ng/ml EGF and 10 ng/ml FGF). After 24 or 48 hours, cells were collected and processed for RNA or protein extraction.

Transient transfections and Luciferase assays were performed in 60% confluent SVZ cell cultures (*CNP*-hEGFR and WT) using NeuroPORTER as described above, and 1.5μg of PGL3 basic, wt phEGFR (Millipore), pCBF1-Luciferase reporter plasmid (gift of Dr. Gabriel Corfas, Harvard Medical School) or *Hes1* Luciferase reporter plasmid, and Dll expression plasmid (gift of Dr. Alanis Israel, Unite de Biologie Moleculaire de l'Expression Genique, Centre National de la Recherche Scientifique) reporter plasmids and 0.3μg of expression vectors. Notch expression vectors used were a kind gift of Dr. Raphael Kopan (Department of Molecular Biology and Pharmacology, Washington University). Luciferase assays were performed 48hr after transfection using the Dual Assay Luciferase kit (Promega). Cotransfected TK–renilla Luciferase was used to normalize samples for transfection efficiency and for sample handling. Cells were lysed, and luciferase activity was measured following the protocol recommended by the manufacturer.

Neural progenitor-neural stem cell co-cultures

NPCs were acutely dissociated from P8 *CNP*-hEGFR and WT SVZ mice and then processed for purification using anti-prominin-1 microbeads antibodies (Miltenyi Biotec, Auburn CA) following manufacturer recommendations. Purified NPCs were cultured at high density in a monolayer in the presence of EGF and bFGF, as described above. After 48 hrs, FACS-purified WT *GFAP*-GFP[+]LeX^{+} cells were plated on top of NPCs for 5 days in EGF- and bFGF-containing medium. Finally, *GFAP*-GFP^{+} cells were purified from the co-culture by FACS and assayed in neurosphere cultures to determine proliferation and self-renewal. FACS-purified *GFAP*-GFP^{+} cells were seeded at a density of 5 viable cells/μl on uncoated 12mm-well plates (BDFalcon, Franklin Lakes, NJ), and maintained in SCM for 6DIV with daily addition of EGF and bFGF. Primary neurosphere colonies were subcloned by mechanical dissociation in SCM with EGF and bFGF. Cells were re-plated at a density of 5 cells/μl on uncoated 24-well plates. Stem cell self-renewal was assessed after further 6 DIV.

Microscopy and cell counting

A Bio-Rad MRC 1024 confocal laser-scanning microscope (Hercules, CA) equipped with a krypton-argon laser and an Olympus IX-70 inverted microscope (Melville, NY) was used to image localization of FITC (488nm laser line excitation; 522/35 emission filter), texas red (568nm excitation; 605/32 emission filter) of Cy5 (647 excitation; 680/32 emission filter). Optical sections (Z=0.5μm) of confocal epifluorescence images were acquire sequentially using a 40x oil objective (Number or aperture, NA=1.35), or a 60x oil objective (NA=1.40) with Bio-Rad *LaserSharp* v3.2 software. *ImageJ NIH,* software was subsequently used to merge images. Merge images were processed in Photoshop 7.0 with minimal manipulations of contrast. For cell counting, cells were counted in the SVZ the postnatal day 8 (P8) and adult mice P90. At least 3 different brains for each strain and each experimental condition were analyzed and counted. Cell counting was performed blindly and tissue sections were matched across samples. The analysis of the SVZ was performed at different anterior-posterior and dorso-ventral levels of the lateral ventricle. An average of 15–20 sections was quantifiedusing unbiased stereological morphometric analysis for the SVZ to obtain an estimate of the total number of positive cells. Then, percentages of cells expressing different antigens were estimated by scoring the number of cells double-labeled with the marker in question. In acute SVZ dissociated cells, 3 coverslips and 8–10 microscopic fields/coverslip were counted from 3 separate cultures. Statistical analysis was performed by unpaired t-test.

Supplementary Material

Refer to Web version on PubMed Central for supplementary material.

Acknowledgments

References

1. Mercier F, Kitasako JT, Hatton GI. Anatomy of the brain neurogenic zones revisited: fractones and the fibroblast/macrophage network. J Comp Neurol. 2002; 451:170–188. [PubMed: 12209835]

2. Alvarez-Buylla A, Lim DA. For the long run: maintaining germinal niches in the adult brain. Neuron. 2004; 41:683–686. [PubMed: 15003168]

3. Doetsch F, Caille I, Lim DA, Garcia-Verdugo JM, Alvarez-Buylla A. Subventricular zone astrocytes are neural stem cells in the adult mammalian brain. Cell. 1999; 97:703–716. [PubMed: 10380923]

4. Palmer TD, Willhoite AR, Gage FH. Vascular niche for adult hippocampal neurogenesis. J Comp Neurol. 2000; 425:479–494. [PubMed: 10975875]

5. Temple S. The development of neural stem cells. Nature. 2001; 414:112–117. [PubMed: 11689956]

6. Sundaram MV. The love-hate relationship between Ras and Notch. Genes Dev. 2005; 19:1825–1839. [PubMed: 16103211]

7. Kumar JP, Moses K. The EGF receptor and notch signaling pathways control the initiation of the morphogenetic furrow during Drosophila eye development. Development. 2001; 128:2689–2697. [PubMed: 11526075]

8. Yoo AS, Bais C, Greenwald I. Crosstalk between the EGFR and LIN-12/Notch pathways in C. elegans vulval development. Science. 2004; 303:663–666. [PubMed: 14752159]

9. Hasson P, et al. EGFR signaling attenuates Groucho-dependent repression to antagonize Notch transcriptional output. Nat Genet. 2005; 237:101–105. [PubMed: 15592470]

10. Hitoshi S, et al. Notch pathway molecules are essential for the maintenance, but not the generation, of mammalian neural stem cells. Genes Dev. 2002; 16:846–858. [PubMed: 11937492]

11. Alexson TO, Hitoshi S, Coles BL, Bernstein A, van der Kooy D. Notch signaling is required to maintain all neural stem cell populations-irrespective of spatial or temporal niche. Dev Neurosci. 2006; 28:34–48. [PubMed: 16508302]

12. Lillien L, Raphael H. BMP and FGF regulate the development of EGF-responsive neural progenitor cells. Development. 2000; 127:4993–5005. [PubMed: 11044412]

13. Breunig JJ, Silbereis J, Vaccarino FM, Sestan N, Rakic P. Notch regulates cell fate and dendrite morphology of newborn neurons in the postnatal dentate gyrus. Proc Natl Acad Sci USA. 2007; 104:20558–20563. [PubMed: 18077357]

14. Aguirre A, Dupree JL, Mangin JM, Gallo V. A functional role for EGFR signaling in myelination and remyelination. Nat Neurosci. 2007; 10:990–1002. [PubMed: 17618276]

15. Aguirre A, Rizvi TA, Ratner N, Gallo V. Overexpression of the epidermal growth factor receptor confers migratory properties to nonmigratory postnatal neural progenitors. J Neurosci. 2005; 25:11092–11106. [PubMed: 16319309]

16. Steiner B, et al. Type-2 cells as link between glial and neuronal lineage in adult hippocampal neurogenesis. Glia. 2006; 54:805–814. [PubMed: 16958090]

17. Doetsch F, Garcia-Verdugo JM, Alvarez-Buylla A. Cellular composition and three-dimensional organization of the subventricular germinal zone in the adult mammalian brain. J Neurosci. 1997; 17:5046–5061. [PubMed: 9185542]

18. Capela A, Temple S. Lex/ssea-1 is expressed by adult mouse CNS stem cells, identifying them as non-ependymal. Neuron. 2002; 35:865–875. [PubMed: 12372282]

19. Aguirre A, Gallo V. Postnatal neurogenesis and gliogenesis in the olfactory bulb from NG2-expressing progenitors of the subventricular zone. J Neurosci. 2004; 24:10530–10541. [PubMed: 15548668]

20. Jablonska B, et al. Cdk2 is critical for proliferation and self-renewal of neural progenitor cells in the adult subventricular zone. J Cell Biol. 2007; 179:1231–1245. [PubMed: 18086919]

21. Gaiano N, Nye JS, Fishell G. Radial glial identity is promoted by Notch1 signaling in the murine forebrain. Neuron. 2000; 26:395–404. [PubMed: 10839358]

22. Mizutani K, Yoon K, Dang L, Tokunaga A, Gaiano N. Differential Notch signalling distinguishes neural stem cells from intermediate progenitors. Nature. 2007; 449:351–355. [PubMed: 17721509]

23. Lim DA, et al. Noggin antagonizes BMP signaling to create a niche for adult neurogenesis. Neuron. 2000; 28:713–726. [PubMed: 11163261]

24. Colak D, et al. Adult neurogenesis requires Smad4-mediated bone morphogenic protein signaling in stem cells. J Neurosci. 2008; 28:434–446. [PubMed: 18184786]

25. Lai K, Kaspar BK, Gage FH, Schaffer DV. Sonic hedgehog regulates adult neural progenitor proliferation in vitro and in vivo. Nat Neurosci. 2003; 6:21–27. [PubMed: 12469128]

26. Kohyama J, et al. Visualization of spatiotemporal activation of Notch signaling: live monitoring and significance in neural development. Dev Biol. 2005; 286:311–325. [PubMed: 16153632]

27. Aguirre A, Gallo V. Reduced EGFR signaling in progenitor cells of the adult subventricular zone attenuates oligodendrogenesis after demyelination. Neuron Glia Biol. 2007; 3:209–220. [PubMed: 18634612]

28. McGill MA, McGlade CJ. Mammalian numb proteins promote Notch1 receptor ubiquitination and degradation of the Notch1 intracellular domain. J Biol Chem. 2003; 278:23196–23203. [PubMed: 12682059]

29. Chapman G, Liu L, Sahlgren C, Dahlqvist C, Lendahl U. High levels of Notch signaling down-regulate Numb and Numblike. J Cell Biol. 2006; 175:535–540. [PubMed: 17116748]

30. Ling BC, et al. Role for the epidermal growth factor receptor in neurofibromatosis-related peripheral nerve tumorigenesis. Cancer Cell. 2005; 7:65–75. [PubMed: 15652750]

31. Wehner T, et al. Bone marrow-derived cells expressing green fluorescent protein under the control of the glial fibrillary acidic protein promoter do not differentiate into astrocytes in vitro and in vivo. J Neurosci. 2003; 23:5004–5011. [PubMed: 12832523]

32. Luetteke NC, et al. The mouse waved-2 phenotype results from a point mutation in the EGF receptor tyrosine kinase. Genes Dev. 1994; 8:399–413. [PubMed: 8125255]

33. Morshead CM, Craig CG. & van der Kooy, D In vivo clonal analyses reveal the properties of endogenous neural stem cell proliferation in the adult mammalian forebrain. Development. 1998; 125:2251–2261. [PubMed: 9584124]

34. Matsuda T, Cepko CL. Controlled expression of transgenes introduced by *in vivo* electroporation. Proc Natl Acad Sci U S A. 2007; 104:1027–1032. [PubMed: 17209010]

35. Galceran J, Sustmann C, Hsu SC, Folberth S, Grosschedl R. LEF1-mediated regulation of Delta-like1 links Wnt and Notch signaling in somitogenesis. Genes Dev. 2004; 18:2718–2723. [PubMed: 15545629]

36. Ohtsuka T, et al. Visualization of embryonic neural stem cells using Hes promoters in transgenic mice. Mol Cell Neurosci. 2006:109–122. [PubMed: 16214363]

37. Kolev V, et al. The intracellular domain of Notch ligand Delta1 induces cell growth arrest. FEBS Lett. 2005; 24:5798–5802. [PubMed: 16225865]

38. Belachew S, et al. Postnatal NG2 proteoglycan-expressing progenitor cells are intrinsically multipotent and generate functional neurons. J Cell Biol. 2003; 161:169–186. [PubMed: 12682089]
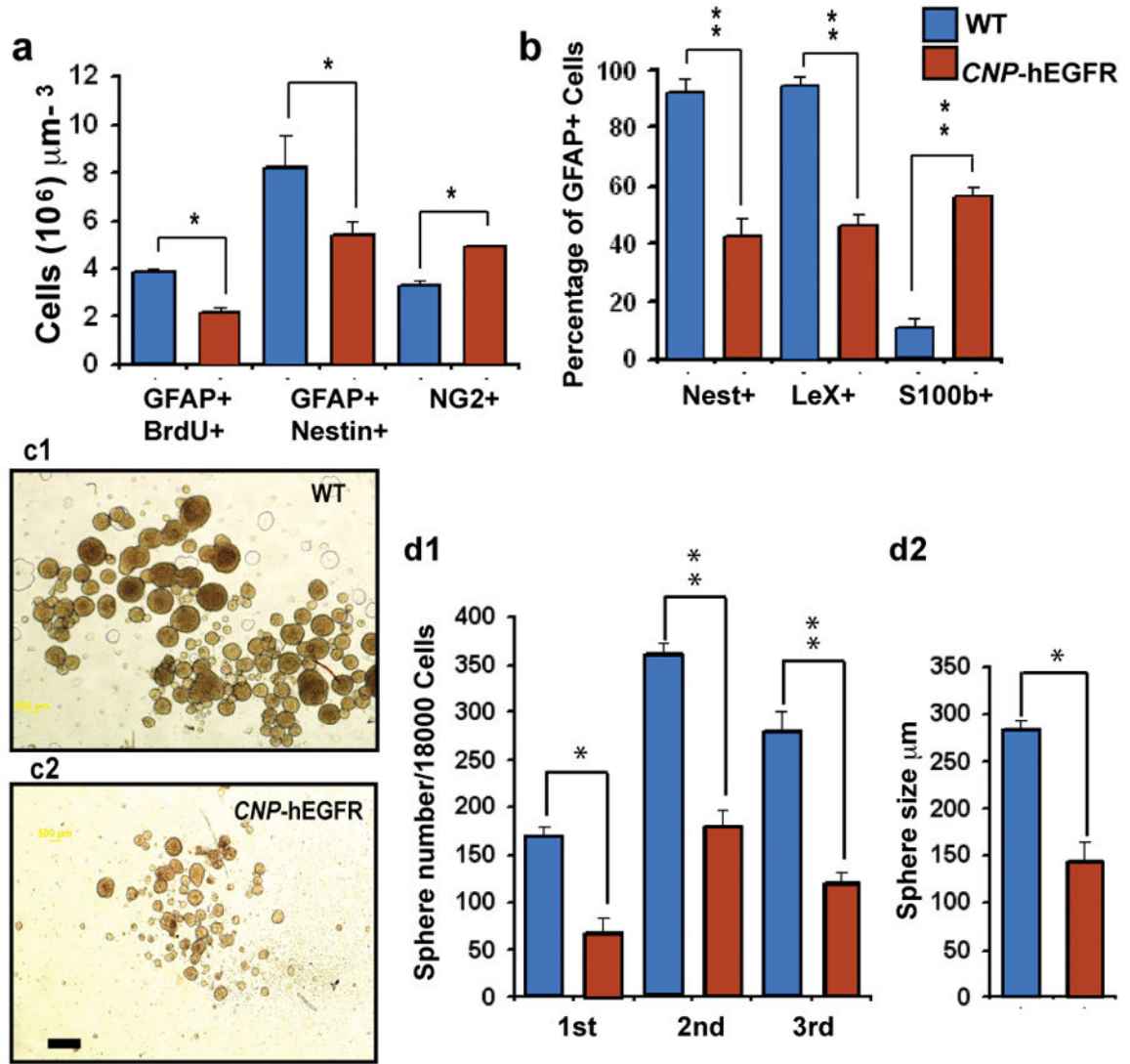
Figure 1. EGFR overexpression reduces NSC proliferation and self renewal in the adult mouse SVZ

(a) Decreased number of GFAP+BrdU+ and GFAP+Nestin+ NSCs, and increased number of NG2+ cells in the SVZ of the *CNP*-hEGFR mouse (*p<0.05). Means ± SEM. (b) Decreased percentage of GFAP+Nestin+LeX+ NSCs and increased percentage of GFAP+S100b+ astrocytes in the SVZ of the *CNP*-hEGFR mouse (**p<0.02). (c) Neurospheres from WT (c1) and *CNP*-hEGFR (c2) cells. (d) Reduced neurosphere numbers (d1) and size (d2) in cultures from *CNP*-hEGFR mice (*p<0.02; **p<0.001).
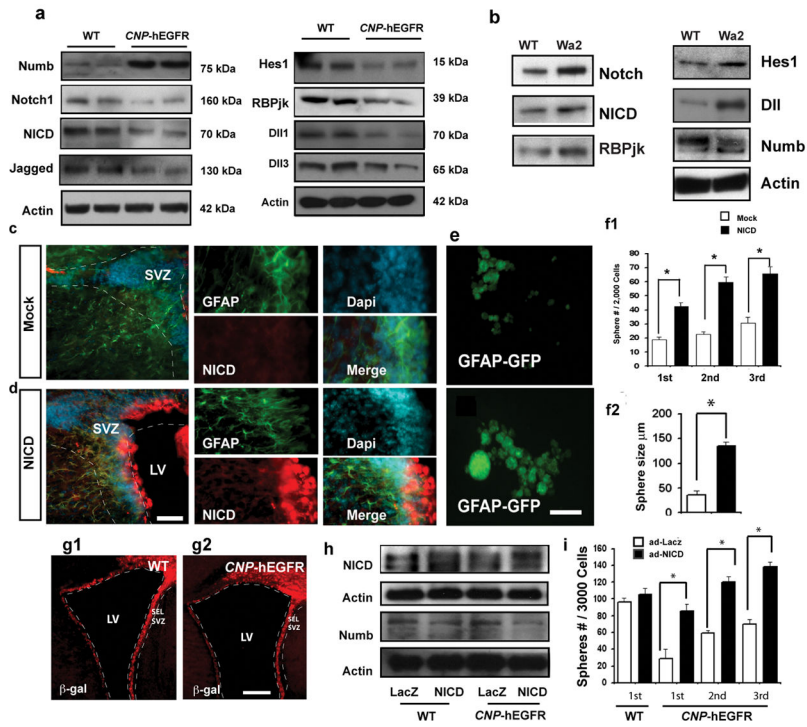
Figure 2. EGFR overexpression downregulates Notch signaling in the SVZ, and NICD overexpression rescues proliferation and self-renewal of SVZ NSCs
(a) Notch signaling is downregulated, but Numb is upregulated in the SVZ of *CNP*-hEGFR mice. (b) NICD, RBPjk, Hes1 are upregulated in the Wa2 SVZ, and Numb is downregulated. (c-d) High NICD levels were detected after in vivo electroporation by immunostaining. (e–f) GFAP-GFP[+] neurosphere number (f1) and size (f2) increased after *NICD* electroporation. Means (n=3) ± SEM (*p<0.01). Scale bars = 100μm. (g) High b-gal expression levels in the SVZ after viral infection in WT (g1) and *CNP*-hEGFR (g2) ventricles. (h) Ad-*NICD* transduction increased NICD, but reduced Numb expression. (i) Ad-*NICD* infection increased neurosphere formation in *CNP*-hEGFR mice, but not in WT. Means (n=3) ± SEM (*p<0.02). Scale bars = 200μm.
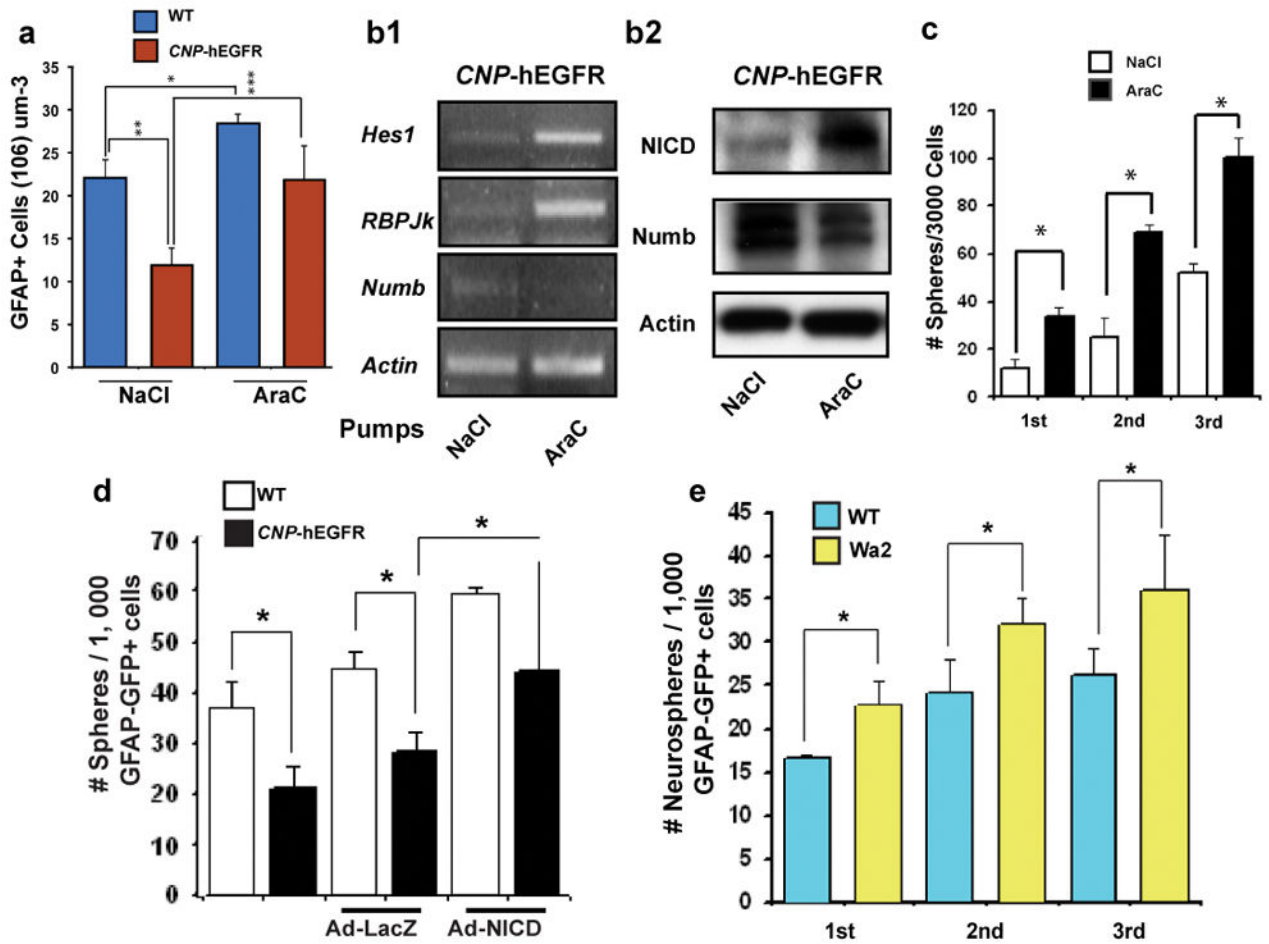
Figure 3. EGFR-expressing NPCs regulate NSC properties through a non-autonomous cellular mechanism

(a) Increased BrdU+ cells and reduced GFAP+ cells in *CNP*-hEGFR mice (**p<0.002). AraC: Increased GFAP+ cells compared with NaCl in *CNP*-hEGFR mice (**p<0.002; *p<0.05). (b1) AraC upregulates *Hes1* and *RBPjk* mRNAs and downregulates *Numb*. (b2) AraC upregulates NICD protein and downregulates Numb. (c) *CNP*-hEGFR mice: AraC increases NSC proliferation and self-renewal (*p<0.001). Means (n=3) ± SEM. (d) Reduced proliferation and self-renewal in WT NSCs cultured with *CNP*-hEGFR NPCs, as compared with WT cells. Ad-*NICD* overexpression rescued NSC proliferation. Means (n=3) ± SEM (*p<0.02). (e) Higher proliferation and self-renewal of NSCs cultured with NPCs of the Wa2 mouse, as compared with WT cells. Means (n=3) ± SEM (*p<0.05).
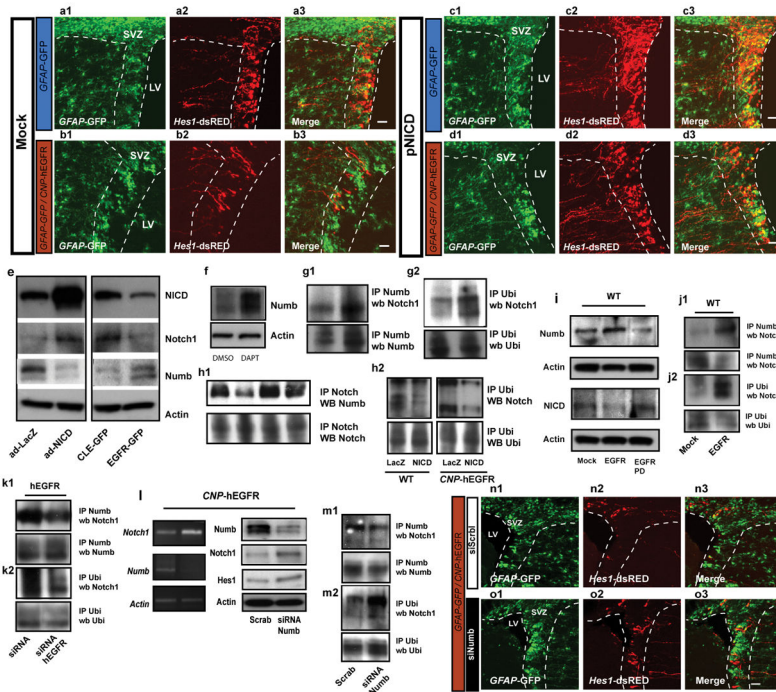
Figure 4. EGFR signaling reduces Notch1 expression through Numb

(a–d) *Hes1*-dsRED-*NICD* co-electroporation in *GFAP*-GFP and *GFAP*-GFP/*CNP*-hEGFR mice. More *Hes1*-dsRED⁺*GFAP*-GFP⁺ cells are observed in *GFAP*-GFP mouse. *NICD* increases *GFAP*-GFP⁺*Hes1*-dsRED⁺ cell number. (e) WT cells infected with: i) LacZ or *NICD*, or ii) GFP retrovirus (*CLE*-GFP) or *EGFR*-GFP. *NICD* upregulates NICD and Notch1, but downregulates Numb. *EGFR* reduces Notch1 and NICD, but increases Numb. (f) DAPT upregulates Numb. (g) Increased Numb/Notch1 immunoprecipitation correlates with enhanced degradation. (h) Ad-*NICD* reduces Notch1/Numb interaction and Notch1 degradation in *CNP*-hEGFR SVZ. (i) *EGFR* increases Numb and reduces NICD; PD168393 prevents these effects. (j) *EGFR* increases Numb/Notch immunoprecipitation, and Notch1 degradation. (k) *hEGFR* siRNAs decrease Numb/Notch1 interaction and Notch1 degradation in *CNP*-hEGFR cells. (l–o) *Numb* siRNA knockdown enhances Notch signaling in *CNP*-hEGFR NSCs. Scrab=scrambled siRNA. (l) *Numb* siRNA downregulates Numb and upregulates Notch1. (m) *Numb* siRNA decreases Numb/Notch interaction and Notch1 degradation. (n–o) Co-electroporation of Scrab or *Numb* siRNA, and *Hes1*-dsRED constructs. *Numb* siRNA increases the number of *Hes1*-dsRED⁺*CAG*-GFP⁺ cells. Scale bar = 50μm.